Applying an artificial neural network to assess thermal transmittance in walls by means of the thermometric method

Abstract

Most of the existing building stock has a deficient energy behaviour. The thermal transmittance of façades is among those aspects which most affect this situation. In this paper, the calculation procedure with correction for storage effects from ISO 9869-1 was applied to the thermometric method to determine the *U*-value. Due to the need for determining the number and type of layers that compose the wall to apply the calculation, a multilayer perceptron has been developed to estimate the *U*-value. From the different model configurations suggested, the most adequate architecture was the one with 14 nodes in the hidden layer without making transformations in the input variables. Valid results have been obtained by the multilayer perceptron for the case studies analysed from different building periods, with deviations lower than 20% between the measured value and the expected one, varying the test duration according to the thermal resistance of the wall and the temperature variations. Furthermore, it is not necessary to carry out a data post-processing for the model, so this fact simplifies and hastens the calculation procedure.

Keywords

Thermal transmittance; thermometric method; thermal mass factors; artificial neural network; multilayer perceptron

Nomenclature

Symbols

C_k: thermal capacity of the layer k [J/(m²·K)]
F_{in}: total internal thermal mass factor [J/(m²·K)]
$F_{in,CCF}$: total internal thermal mass factor using thermal resistance values corrected by CCF [J/(m²·K)]
$F_{in,k}$: internal thermal mass factor for each layer k of the wall [J/(m²·K)]
$F_{Mcorrection}$: moisture correction factor [dimensionless]
F_{out}: total external thermal mass factor [J/(m²·K)]
$F_{out,CCF}$: total external thermal mass factor using thermal resistance values corrected by CCF [J/(m²·K)]
$F_{out,k}$: external thermal mass factor for each layer k of the wall [J/(m²·K)]
$F_{Tcorrection}$: temperature correction factor [dimensionless]
h_{in}: total internal heat transfer coefficient [W/(m²·K)]
q_j: specific heat flux through the element at the instant j [W/m²]
R: thermal resistance of the wall [(m²·K)/W]
R_{CCF}: thermal resistance of the material by applying the CCF correction [(m²·K)/W]
$R_{in,k}$: sum of the internal thermal resistances from the k-1th layer to the internal air [(m²·K)/W]
R_k: thermal resistance of the layer k [(m²·K)/W]
$R_{out,k}$: sum of the external thermal resistances from the k+1th layer to the external air [(m²·K)/W]
s: thickness [m]
$T_{in,j}$: internal air temperature at the instant j [K]
$T_{out,j}$: external air temperature at the instant j [K]
$T_{s,in,j}$: internal surface temperature of the wall at the instant j [K]
U: thermal transmittance [W/(m²·K)]
U_{THM}: thermal transmittance obtained by the thermometric method [W/(m²·K)]
$U_{\mathrm{THM,Fk}}$: thermal transmittance obtained by the thermometric method with correction for storage effects [W/(m²·K)]
$U_{\mathrm{THM,MLP,Fk}}$: thermal transmittance obtained by the multilayer perceptron [W/(m²·K)]
$w_{10}^{(2)}$: weight of the bias neuron of the hidden layer of the multilayer perceptron
$w_{ji}^{(1)}$: weights of the hidden layer of the multilayer perceptron
$w_{kj}^{(2)}$: weights of the output layer of the multilayer perceptron
x_i: values of the input layer of the multilayer perceptron
y_0: input value of the bias neuron of the hidden layer of the multilayer perceptron
z_k: output of the final layer of the multilayer perceptron

Greek symbols

Δt: time interval between the measurements [s]
δT_{in}: difference between the average internal air temperature from the 24 h before measuring the observation and the

average internal air temperate from the first 24 h of the test [K]
δT_{out}: difference between the average external air temperature from the 24 h before measuring the observation and the average external air temperature from the first 24 h of the test [K]
λ: thermal conductivity [W/(m·K)]
σ: activation function of the multilayer perceptron

Abbreviations
ANN: artificial neural networks
AVRA: Agency for Housing and Rehabilitation in Andalusia
BFGS: Broyden-Fletcher-Goldfarb-Shanno algorithm
BP: back propagation
CCF: conductivity correction factors
CTE: Spanish Technical Building Code
ECM: energy conservation measure
MAE: mean absolute error
MLP: multilayer perceptron
MW: mineral wool
P: building period
P1: building period anterior to NBE-CT-79
P2: building period between NBE-CT-79 and CTE
P3: building period posterior to CTE
PUR: polyurethane
R^2: linear correlation coefficient
RMSE: root mean square error
THM: thermometric method
XPS: extruded polystyrene

1. Introduction

Society is more and more aware of the effect that everyday processes have on nature, causing the acceleration of global warming, climate change and the extinction of different species [1]. One of the fundamental aspects which would change this situation is the reduction of greenhouse gas emissions. Recently, the European Union has published a roadmap for moving to a low carbon economy with the aim of reducing pollutant gas emissions by 80% by 2050 [2]. To achieve this, it is estimated that the building sector should cut its emissions by 90% due to its high energy consumption [2]. In this sense, from the different activities and procedures carried out nowadays, residential buildings were responsible for 24.79% of the total primary energy consumption in Europe in 2014 [3]. The main consumption source in these buildings is the heating [4]. Therefore, it is necessary to cut the level of the greenhouse gas emissions by reducing the energy demand from the existing building stock. Within this context, the adoption of the energy conservation measures (ECMs) in old buildings is one of the most significant performances [2]. In order to configurate correctly the ECMs, it is essential to determine the thermal transmittance (*U*-value) of the envelope [5,6], since it usually exceeds the maximum admissible levels from the technical standard in most cases [7] and has a major impact on façades, in which the maximum admissible value of energy loss can be exceeded by more than 100% [8].

The determination of thermal transmittance can be carried out by both theoretical and experimental methods. The theoretical method is included in ISO standard 6946 [9], and it calculates thermal transmittance of a conventional wall through the thickness and the thermal conductivity of each of its layers, as well as the internal and external surface thermal resistances. It is a method with a high uncertainty level, since it is difficult to know accurately the layers of the wall unless an endoscopic analysis can be carried out [10] or technical data are available [11]. Regarding experimental methods, in scientific literature there is the heat flow meter method included in ISO 9869-1 [12] as well as quantitative methods of infrared thermography, with different approaches from both exterior and interior [13].

Recently, Andújar Márquez et al. [14], Bienvenido-Huertas et al. [15], and Kim et al. [16] validated the use of the thermometric method (also known as air–surface temperature ratio method) to determine the *U*-value by means of in situ tests. This method differs from the heat flow meter method in that the heat flux is not measured, but the internal surface temperature of the wall. However, no using the heat flux plate does not affect the representation of results, as differences lower than 5% between the thermometric method and the heat flow meter method can be obtained in steady state conditions [16].

Obtaining thermal transmittance value by means of the measurement using temperature sensors can reduce the error associated with the test because of putting the heat flux plate. In this sense, Meng et al. [17] determined that the maximum error due to the use of surface temperature probes in the U-value is of 6%, whereas using the heat flux plate increases the maximum error to 26%. Regarding the thermometric method (THM), another aspect to highlight is the fact that no using the plate avoids the disturbance that probe can cause to thermal behaviour of the wall [10,18]. With respect to infrared thermography methods, THM has the advantage of not being significantly influenced by the environmental factors. In this sense, the influence of input variables on the results of infrared thermography methods is very significant, leading to obtain atypical results [19,20]. Moreover, variations of 50% in the measurement of internal, external, and surface air temperature can lead to errors of 5%, 50%, and 50%, respectively [19], whereas a deviation of 1 °C in the measurement of the reflected temperature can cause errors up to 100% [21].

For walls with a high thermal resistance, the thermal storage effect should be considered [12]. The thermal mass is the capacity to store thermal energy, that is, the effect that the components with a large heat capacity can produce in order to alleviate the temperature oscillations and reduce the rate of change [22]. The thermal storage characteristics and the material transmission of a component should be studied as a complete system, since any material influences the other [23].

The high thermal mass of walls limits the use of experimental methods [24]. The fundamental limitation of experimental methods is that the change of amount of heat stored in the wall is required to be low in comparison with the amount of heat going through it [25]. However, this requirement is difficult to achieve, especially in less cold climate regions [26]. In scientific literature, there are studies analysing the application of the heat flow meter method in high thermal mass buildings with significant deviations in the results obtained. Asdrubali et al. [27] assessed the thermal transmittance of six walls with a high thermal resistance using the ISO standard 9869-1. Results obtained deviations up to 75% for the case studies analysed. Nardi et al. [28] evaluated two walls with low thermal transmittance values, obtaining deviations between 47 and 83% in the results. Samardzioska and Apostolska [29] analysed the thermal transmittance of a constructive system (Fragmat NZ-1) in three different walls. Results obtained deviations lower than 25%, although authors excluded certain monitored days, since the required conditions of data analysis were not achieved. Gaspar et al. [30] determined that steady state conditions with temperature differences higher than 19 °C can lead to obtain results with deviations of 1.9%, although it is difficult to guarantee this thermal gradient in actual conditions.

Traditionally, the different steady state methods try to limit the thermal storage effect by extending the test duration to at least 72 h, and in some cases more than two weeks [31]. Duration is influenced by the wall typology. In this sense, Ficco et al. [32] determined that the sample period should be extended for those elements with a high thermal inertia, particularly in unfavourable conditions, such as a low thermal gradient or heat flow inversions. These test durations cause an excessive consumption of time resources as well as disturbances for dwellings´ tenants [33], and do not guarantee the limitation of thermal storage effect [34]. In this sense, Bienvenido-Huertas et al. [15] showed the difficulties to obtain representative results using THM when steady state conditions were not achieved during the tests. Kim et al. [35] indicated that thermal resistance values of walls and the difficulty in guaranteeing steady state conditions could make the correct estimation of test durations difficult in order to obtain representative results for THM, so the deviation of the result obtained can be high.

The data analysis methodology used plays an important role. According to Cesaratto and Carli [36], the accuracy of thermal transmittance results could cause variations higher than 20%, depending on the method employed. A theoretical methodology to determine the *U*-value considering this effect is described in section 7.2. from ISO 9869-1. In this methodology, it is necessary to know the thermal characteristics of the layer components. Deconinck et al. [25] determined that using this methodology reduced test durations for the heat flow meter method. In this line, Choi and Ko [37] stated that test duration was reduced to two days by using this method, obtaining more accurate results than the average method. Thus, implementing this methodology for THM can be an opportunity to analyse walls with high thermal mass. Nevertheless, the composition of the wall is unknow in most cases [32], since a reliable technical documentation is not available or an endoscopy cannot be made. So, it is essential to have data analysis techniques that allow to determine the *U*-value of a wall without knowing exactly its layers to apply the corrections for storage effects. In this sense, the regression techniques have become very important to estimate thermal transmittance.

From the different existing regression techniques, artificial neural networks (ANNs) are one of the typologies ensuring greater reliability and viability [38]. ANNs imitate the hardware structure of the nervous system with the aim of building parallel and adaptive processing information systems which can estimate an efficient response. Along with the Expert Systems, ANNs are one of the study gaps on artificial intelligence in the last years [39]. In the field of building energy problems, they have been widely used with correlation coefficients and error values adequate for each case [40]. Moreover, they have been extensively used as a prediction tool of energy demand and consumption [41], although other researches focused on the characterisation of the thermal properties of components can be highlighted, such as: (i)

Chudzik [42] applied an ANN to determine the heat transfer coefficient on the specimen surface to establish the thermal properties of thermal insulating materials; (ii) an ANN was designed by Buratti et al. [43] to predict the *U*-value of wooden windows; (iii) Sablani et al. [44] designed two ANN models to estimate the heat transfer coefficient for a liquid-solid set through its internal temperature; (iv) Singh et al. [45] determined the effective thermal conductivity of porous materials filled with different liquids using ANNs; and (v) Mitra et al. [46] predicted the thermal resistance of handloom cotton fabrics using an ANN. However, all these researches used fixed values for the input variables of ANNs, so ANNs were not used as a data analysis method for time series obtained by monitoring an element.

Therefore, this paper is aimed at filling the existing gap in the state of the art. A new data analysis method is suggested for the thermometric method by means of an ANN allowing to characterise thermal transmittance of walls, considering the effect of thermal storage and without having the need of knowing the exact composition of the wall (fundamental requirement to carry out the calculation procedure).

This article gives a new approach to deal with data analysis limitations to determine the thermal transmittance existing in scientific literature, suggesting an efficient methodology to be applied in order to characterize the U-value of walls. In addition, aspects never discussed in scientific literature are suggested, such as using ANNs as data analysis methodology to determine thermal transmittance and implementing a calculation methodology with correction for storage effects for THM. The key contributions of this paper can be briefly summarized as follows:

- Applying the calculation procedure with correction for storage effects for THM.
- Developing and analysing ANN models to determine thermal transmittance with correction for storage effects without the need of previously knowing the thermophysical properties of the materials of the wall.
- Determining limitations to assess thermal transmittance by means of the model developed, analysing the time required and the need of performing a post-processing.
- Proposing a new data analysis methodology obtained for THM, as well as assessing the potential of using ANNs as data analysis methodology to quantify thermal transmittance.

This article starts by explaining the basis of the calculation methodology of THM in section 2. Section 3 details the design of both ANN models developed in this research. Then, Section 4 describes training and testing datasets used in this study. Section 5 analyses and discusses the calculation procedure, the ANN architecture and model with the best behaviour as well as the applicability of this model to new case studies. Finally, section 6 sums up the main conclusions of this study.

2. Theory and calculation methods

2.1. Average method

The theoretical framework of THM is explained in detail in the publications by Andújar Márquez et al. [14], Bienvenido-Huertas et al. [15], and Kim et al. [16]. Therefore, a brief description of the equations is given in this section.

THM is based on the average method from ISO 9869-1 [12]. In this standard, the thermal transmittance of an element is defined as the heat flux that goes through the element divided by the difference between the internal and external air temperatures under the conditions of a stationary regime [12], and it is obtained as follows:

$$U = \frac{\sum_{j=1}^{n} q_j}{\sum_{j=1}^{n}\left(T_{in,j} - T_{out,j}\right)} \left[\frac{\mathrm{W}}{\mathrm{m^2 \cdot K}}\right] \quad (1)$$

Where q_j [W/m²] is the specific heat flux through the element at the instant *j*, and $T_{in,j}$ and $T_{out,j}$ [K] are the internal and external air temperature at the instant *j*, respectively.

THM applies Newton's Law of Cooling provided that the wall is the area of heat transfer (Eq. (2)). Considering that the heat transfer by conduction is the same as the heat transfer by convection and radiation in steady state (Eq. (3)), Eq. 4 is obtained following the progressive average procedure to determine the *U*-value.

$$q = h_{in}(T_{in} - T_{s,in}) \left[\frac{\mathrm{W}}{\mathrm{m^2}}\right] \quad (2)$$

$$U(T_{in} - T_{out}) = h_{in}(T_{in} - T_{s,in}) \left[\frac{\mathrm{W}}{\mathrm{m^2}}\right] \quad (3)$$

$$U = \frac{\sum_{j=1}^{n}\left(h_{in}\left(T_{in,j} - T_{s,in,j}\right)\right)}{\sum_{j=1}^{n}\left(T_{in,j} - T_{out,j}\right)} \left[\frac{\mathrm{W}}{\mathrm{m^2 \cdot K}}\right] \quad (4)$$

Where h_{in} [W/(m²·K)] is the total internal heat transfer coefficient, and $T_{s,in,j}$ [K] is the internal surface temperature of the wall at the instant *j*.

Thus, the way to obtain the thermal transmittance is by measuring, on the one hand, the external and internal air temperatures and, on the other hand, the internal surface temperature. Hence, the measurement errors associated with the use of the heat flux plate are avoided [15]. For h_{in}, the reciprocal of the tabulated value of internal surface resistance established in ISO 6946 [9] is used, being 7.69 W/(m²·K) the value associated for façades. This value is obtained by the mechanisms of heat transfer by convection and radiation, with a value of 2.5 W/(m²K) for the convective heat transfer coefficient and a value of 5.19 W/(m²K) for the radiative heat transfer coefficient [47], being applicable to surfaces with a medium-high emissivity [9]. Thus, it is applied to most of the buildings, since values of emissivity of most materials used in the façades are between 0.90 and 0.96 [48].

It is important to highlight that, from the two heat transfers which define the total internal heat transfer coefficient, transfer by convection is the one that has a less rigorous development, existing a wide variety of expressions for correlation coefficients due to temperature differences, wind speeds or dimensionless numbers [49]. In this sense, the value from ISO 6946 has a behaviour similar to the convective heat transfer coefficient proposed by Khalifa and Marshall [50], with deviations lower than 6% [47], whereas deviations can reach 20% for other correlations. In a recent study, Kim et al. [35] analysed the use of the value of h_{in} from ISO 6946 for THM. Tests obtained deviations lower than 5% with respect to the heat flow meter method, so this value is the most adequate with respect to other correlation values or coefficients existing in scientific literature [35]. Furthermore, the use of this value allows to establish linear correlations between the difference of internal and external air temperatures as well as the difference of internal surface temperature and internal air temperature for each *U*-value (see Fig. 1), making the behaviour of the input variables for each value of the thermal transmittance more understandable in the same way that for the heat flow meter method (Eq. (1)).

Fig. 1. Relation between the difference of internal and external air temperatures (x-axis), and the difference of internal air temperature and the internal surface temperature of the wall (y-axis) for an internal convective coefficient of 7.69 [W/(m²·K)].

The use of the average method requires the change of the heat stored in the wall to be insignificant in comparison with the heat that goes through the wall, so the test duration should last between 3 and 14 days. However, there are difficulties to fulfil those conditions, such as [35,51]: (i) oscillations in temperature values and difficulties to achieve steady state conditions; (ii) the time needed to carry out the tests; (iii) significant variations in the convective heat flux due to operation cycles of heating systems; and (iv) putting the tenants of the analysed dwellings to great inconvenience. Thus, an improvement in the calculation procedure, where the thermal mass of the wall is taken into account, allow to reduce the error of the obtained result as well as to shorten the period of test performance [37].

2.2. Average method with correction for storage effects

The standard of the heat flow meter method [12] establishes a calculation procedure of thermal transmittance by correcting the heat storage effects for walls having both high resistance values and thermal mass. This calculation procedure should be applied when the *U*-value obtained at the end of the test varies more than 5% with respect to the value obtained 24 h before or to the data from the first two days [12]. To apply this procedure, it is fundamental to know the thermal characteristics of the layers composing the wall with the aim of also knowing its thermal resistance (Eq. (5)) and thermal capacity.

$$R = \frac{s}{\lambda}\left[\frac{\mathrm{m}^2 \cdot \mathrm{K}}{\mathrm{W}}\right] \tag{5}$$

Where s [m] and λ [W/(m·K)] are the thickness and the thermal conductivity of the material, respectively.

For each layer k of the wall, the thermal resistance is calculated, and the internal and external thermal mass factor are obtained (Eqs. (6) and (7)).

$$F_{out,k} = C_k\left[\frac{R_k}{R}\left\{\frac{1}{6} + \frac{R_{in,k} + R_{out,k}}{3R}\right\} + \frac{R_{in,k}R_{out,k}}{R^2}\right] \tag{6}$$

$$F_{in,k} = C_k\left[\frac{R_{out,k}}{R} + \frac{{R_k}^2}{3R^2} - \frac{R_{in,k}R_{out,k}}{R^2}\right] \tag{7}$$

Where $R_{out,k}$ [(m²·K)/W] is the sum of the external thermal resistances from the k+1th layer to the external air, $R_{in,k}$ [(m²·K)/W] is the sum of the internal thermal resistances from the k-1th layer to the internal air, $F_{out,k}$ [J/(m²·K)] is the external thermal mass factor of the layer k, $F_{in,k}$ [J/(m²·K)] is the internal thermal mass factor of the layer k, C_k [J/(m²·K)]

is the thermal capacity of the layer k, R_k [(m²·K)/W] is the thermal resistance of the layer k, and R [(m²·K)/W] is the thermal resistance of the wall.

Thermal mass factors of the wall are obtained by means of the sum of thermal mass factors of the N layers of the wall:

$$F_{in} = \sum_{k=1}^{N} F_{in,k} \tag{8}$$

$$F_{out} = \sum_{k=1}^{N} F_{out,k} \tag{9}$$

Where F_{in} [J/(m²·K)] is the total internal thermal mass factor, and F_{out} [J/(m²·K)] is the total external thermal mass factor.

To apply the correction, the numerator from Eq. 1 should be replaced by the following expression:

$$\sum_{j=1}^{n} q_j - \frac{(F_{in}\delta T_{in} + F_{out}\delta T_{out})}{\Delta t} \tag{10}$$

Where δT_{in} [K] is the difference between the average internal air temperature from the 24 h before measuring the observation and the average internal air temperate from the first 24 h of the test, δT_{out} [K] is the difference between the average external air temperature from the 24 h before measuring the observation and the average external air temperature from the first 24 h of the test, and Δt [s] is the time interval between the measurements.

Considering that the heat flux density of an element is equivalent to the density transferred from the internal air to the surface of the element analysed (Eq. (2)), Eq. (10) can be modified:

$$\sum_{j=1}^{n} \left(h_{in}\left(T_{in,j} - T_{s,in,j}\right)\right) - \frac{(F_{in}\delta T_{in} + F_{out}\delta T_{out})}{\Delta t} \tag{11}$$

This expression (Eq. (11)) is applied to Eq. (4), obtaining the following equation:

$$U = \frac{\sum_{j=1}^{n} \left(h_{in}\left(T_{in,j} - T_{s,in,j}\right)\right) - \frac{(F_{in}\delta T_{in} + F_{out}\delta T_{out})}{\Delta t}}{\sum_{j=1}^{n}\left(T_{in,j} - T_{out,j}\right)} \left[\frac{\mathrm{W}}{\mathrm{m^2 \cdot K}}\right] \tag{12}$$

Therefore, the method applies a correction factor which increases or reduces the numerator from Eq. (4) according to the variations of the average internal and external temperatures.

Determining the composition of the wall can be carried out by several techniques, such as the analogy of similar constructions [11], the endoscopy [52], or the use of reliable technical documentation [11]. As there are difficulties to access to the project details as well as the impossibility of making an endoscopy due to the havoc caused in the wall, determining the configuration of the wall by means of either the analogy of similar constructions or based on previous experiences is the technique most used in most professional cases [11], although the associated error is high.

2.3. Average method with correction for storage effects using CCF

The thermal conductivity does not always coincide with the tabulated values included in technical catalogues and projects, since it can vary depending on the environmental temperature and moisture [53]. Most database establish average temperature and moisture conditions to carry out the calculation procedure of thermal conductivity from ISO 10456 [54]. Due to this, Pérez-Bella et al. [55] achieved conductivity correction factors (*CCF*) for each of the province capitals in Spain according to the external ambient conditions. *CCF* can simplify the application of ISO 10456 by combining a temperature conversion factor and a moisture conversion factor (Eq. (13)), both applied to the thermal conductivity of the material with the result of obtaining a more representative thermal resistance (Eq. (14)).

$$CCF = F_{Tcorrection} \cdot F_{Mcorrection} \tag{13}$$

$$R_{CCF} = \frac{s}{\lambda \cdot CCF} \left[\frac{\mathrm{m^2 \cdot K}}{\mathrm{W}}\right] \tag{14}$$

Where CCF [dimensionless] is the conductivity correction factor for a certain province capital in Spain published by Pérez-Bella et al. [55], $F_{Tcorrection}$[dimensionless] is the temperature correction factor, $F_{Mcorrection}$ [dimensionless] is the moisture correction factor, and R_{CCF} [(m²·K)/W] is the thermal resistance of the material by applying *CCF* correction.

So, Eq. (12) can be modified by using thermal mass factors, which are modified by applying *CCF* to the province capital where tests are performed. Thus, the following expression is obtained:

$$U = \frac{\sum_{j=1}^{n}\left(h_{in}\left(T_{in,j} - T_{s,in,j}\right)\right) - \frac{\left(F_{in,CCF}\delta T_{in} + F_{out,CCF}\delta T_{out}\right)}{\Delta t}}{\sum_{j=1}^{n}\left(T_{in,j} - T_{out,j}\right)} \left[\frac{\mathrm{W}}{\mathrm{m^2 \cdot K}}\right] \quad (15)$$

Where $F_{in,CCF}$ [J/(m²·K)] and $F_{out,CCF}$ [J/(m²·K)] are the total internal and external thermal mass factor using thermal resistance values corrected by *CCF*, respectively.

3. Estimation of *U*-value using ANN

To apply the proposals of the average method with correction for storage effects (Eqs. (12) and (15)), a previous knowledge or a good estimation of thickness, thermal conductivity, and thermal capacity of the layers of the wall are required to calculate thermal mass factors. As mentioned above, consulting project details or making endoscopies are the most adequate methods to know the thermal properties of the wall, but these options are not always possible, and it is necessary to resort to the estimation by means of either the analogy of similar constructions or based on previous experiences.

For this reason, it is essential to have analysis techniques predicting thermal transmittance taking into account the thermal storage effect of the wall and without having the need of knowing its constructive composition. From the different existing typologies to perform an advanced data analysis, ANNs are the ones which best features have [38], and the multilayer perceptron (MLP) is the most used structure.

The MLP structure is formed by three or more layers: an input layer, one or several hidden layers, and an output layer. In each layer, there are neurons or nodes connected to those of the following layer by means of weighted connection with different weights. The neurons of the input layer do not make any calculation but send information. Each neuron of the hidden layer adds all the inputs together, so if that value is higher than the activation value, an output is produced. The outputs go over to the output layer where the process is repeated, and the system response is obtained. The MLP operation is mathematically expressed as follows:

$$z_k = \sigma\left(\sum_{j=1}^{M} w_{kj}^{(2)}\sigma\left(\sum_{i=0}^{d} w_{ji}^{(1)}x_i\right) + w_{10}^{(2)}y_0\right) \quad (16)$$

Where z_k is the output of the final layer, $w_{kj}^{(2)}$ are the weights of the output layer, σ is the activation function, $w_{ji}^{(1)}$ are the weights of the hidden layer, x_i are the values of the input layer, and $w_{10}^{(2)}$ and y_0 are the weight and the input value of the bias neuron of the hidden layer, respectively.

To ease the understanding of the steps followed in the research, Fig. 2 shows the flow-chart representing the main steps of the research.

Fig. 2. Flow-chart of the procedure followed in the research.

3.1. Phase 1. Design and data collection

The design of MLPs with two or more hidden layers does not usually generate a better behaviour of the model, increasing the risk of converging to a local minima [56]. For this study, the authors proposed three layers as architecture for the MLP (see Fig. 3). The MLP estimated the *U*-value of the wall by means of the time series of internal (T_{in}) and external air temperatures (T_{out}), and the internal surface temperature ($T_{s,in}$). Other variables required to characterise thermal transmittance were the average difference temperatures from the first 24 h, both internal (δT_{in}) and external (δT_{out}), as well as the thickness of the wall (s), the time interval between the measurements (Δt), and the building period (P). Regarding this last variable, the most predominant construction typologies in Spain (from the middle of the 20 century to nowadays) can be divided into three building periods [57]: (i) anterior to the normative NBE-CT-79 [58]; (ii) posterior to NBE-CT-79, and anterior to the Spanish Technical Building Code (CTE) [59]; and (iii) posterior to CTE. Buildings constructed anterior to NBE-CT-79 are characterised by being formed by one or two brick layers, without insulation and with the possibility of having an air gap [7], while with NBE-CT-79 coming into force, insulating material was added to the constructive solutions with thicknesses lower than 3 cm [60]. The implementation of CTE increased the limit values of thermal resistance, so the insulation thickness of the buildings from this period is higher [60]. With respect to data input, three discrete values were used for this variable: *P1* (anterior to NBE-CT-79), *P2* (between NBE-CT-79 and CTE), and *P3* (posterior to CTE). This can be quickly determined by consulting the cadastral data of the building.

Considering the existing linear correlations between the temperature differences for each thermal transmittance value (Fig. 1), another MLP was developed by transforming the variables T_{in}, T_{out} and $T_{s,in}$ into the difference of internal and external air temperature ($T_{in} - T_{out}$), and the difference of internal air temperature and internal surface temperature ($T_{in} - T_{s,in}$). Therefore, two MLPs were designed: MLP1 for temperature variables without being modified and MLP2 for transformed variables (see Fig. 3).

Fig. 3. Schematic diagram of the MLPs designed.

3.2. Phase 2. Training and validating the MLP, and selecting the best architecture

The MLP was trained by back propagation (BP) [61]. The Quasi-Newton Method was used as algorithm of second order, using Broyden-Fletcher-Goldfarb-Shanno (BFGS) [62] updates due to the high accuracy achieved by both of them in results [63]. Test data indicated in section 4 of this paper were used as training and testing dataset. For both hidden and output layer, a sigmoidal activation function was used.

During the training, input data had the correct *U*-value as classification value. The result of the MLP depends on the number of neurons of the hidden layer. Therefore, to obtain an optimal result, the numbers of neurons generating a better behaviour should be analysed [40]. For this reason, architectures of the MLP in which the number of neurons in the hidden layer oscillated between 4 and 15 were analysed. Furthermore, a momentum of 0.2 and a learning rate of 0.3 were used as fixed parameters. The number of training time was between 500 and 120,000 until determining the optimal configuration, using a 10-fold cross validation. The assessment of the correct number of nodes from the hidden layer as well as the performance of the MLP were determined by the linear correlation coefficient (R^2) (see Eq. (17)), the mean absolute error (*MAE*) (see Eq. (18)), and the root mean square error (*RMSE*) (see Eq. (19)). The use of these parameters was useful to determine efficiently the performance of the models [64]. Both *MAE* and *RMSE* should be as small as possible, whereas R^2 should have values close to 1, since its value scale goes from 0 (null correlation) to 1 (total correlation) [38]. The determination of the nodes composing the hidden layer to achieve an optimal performance is discussed in the result section of this paper.

$$R^2 = 1 - \frac{\sum_{i=1}^{n}(y_i - x_i)^2}{\sum_{i=1}^{n} x_i^2} \tag{17}$$

$$MAE = \frac{\sum_{i=1}^{n}|y_i - x_i|}{n} \tag{18}$$

$$RMSE = \left(\frac{\sum_{i=1}^{n}(y_i - x_i)^2}{n}\right)^{1/2} \tag{19}$$

Where n is the number of observations in the training dataset, y_i is the value predicted by the ANN, and x_i is the measured value.

3.3. Phase 3. Comparing models and testing the model selected in new case studies

After determining the most optimal architectures of MLP1 and MLP2, the behaviour of both models was compared using the statistical parameters of R^2, *MAE* and *RMSE*. Then, the MLP with the most adequate behaviour was determined, and three new case studies no included in the training process were used for testing its behaviour in new case studies belonging to the three building periods considered.

4. Experimental campaign and dataset used

To do the training and the testing, a dataset composed by 69 subsets was used. Each of these subsets corresponded to tests carried out in different façades. The façades analysed were common wall typologies from the three building periods considered: *P1*, *P2* and *P3.* The façades were multilayer walls with brick leaves, with or without insulation. It is a constructive typology widely used in several countries like Belgium [65], United Kingdom [66] or Italy [67], so the application of the data analysis method can be extended to other regions. Some of the tests were performed by the authors and the others by the Agency for Housing and Rehabilitation in Andalusia (AVRA) of the Regional Government of Andalusia under the Energy Improvement in the Public Housing Stock Program. Choosing the walls, selecting the equipment and mounting the probes were done according to the methodology described by Bienvenido-Huertas et al. [15]. Tests were

performed between 4 and 7 days, with a data acquisition interval of 15 minutes, and each measured instant of time was an observation of the subset. Observations from the first 24 h of each test were not included in the subsets generated. For each wall, there was a reliable technical documentation which allowed to determine the number, the material and the thickness of their layers exactly. The values of thermal conductivity and capacity were obtained from the constructive elements catalogue in Spain for the different materials [68]. Tests were performed in the locations of Cadiz, Cordoba, Granada, Huelva, Jaen, Malaga, and Seville, so the value of the used *CCF* varies (see Table 1).

Table 1
CCF for the locations of the analysed walls.

As indicated in section 3, from the 69 tests available, 66 were used for training and validating the MLPs, and therefore determining which method was the most adequate (see Fig. 4). Data included in subsets corresponded to input data from the MLP as well as to the classification value (see Table 2). With respect to the three new case studies included in the testing of the model selected, Table 3 and Fig. 4. show the sketch, technical characteristics and thermophysical properties of each one.

Table 2
Input and output data compiled in datasets for both models of MLP.

Table 3
Technical characteristics and thermophysical properties of the walls used for testing the MLP.

Fig. 4. Scheme of the training and testing of the MLP.

5. Results and discussion

First, the results obtained for the training dataset of the MLP were analysed with the aim of studying the limitations of Eqs. (12) and (15). It is important to highlight that all the tests included in the training dataset of the neural network had thermal transmittance values without correction (Eq. (4)) and with differences higher than 5% with respect to the observations from the previous 24 h, being in some cases higher than 30%. Table 4 shows the values obtained for Eqs. (4), (12), and (15) in two walls from each building period. These equations were applied to the data obtained in 2 and 3 days. Furthermore, the estimated value of thermal transmittance was obtained by applying ISO 6946 in order to determine the percentage error of the result obtained by the test, following the validation criteria from ISO 9869-1 [12]. As mentioned above, a precise technical documentation was acquired, so it was possible to determine exactly the dimensions and thermal properties of the materials composing the walls analysed. The uncertainty of the obtained results was determined by the combined standard uncertainty from ISO/IEC Guide 98-3 [69].

Table 4
Results obtained of some of the walls of the training dataset.

By analysing the results, it was detected that the *U*-value corrected in the walls from *P1* had results more approximate to the estimated value, with errors lower than 10%. Generally, the values obtained in THM without correction in the façades from this period were adequate because they presented a difference lower than 20% with respect to the estimated value. However, using correction for storage effects could reduce the deviation percentage. Regarding the walls from *P2* and *P3*, the application of correction could reduce the deviation percentage in comparison with the method without correction in most cases. In the examples included in Table 4, the application of correction allowed to reduce the obtained error from 32% to 13% and from 5% to 4% for the data analysed in the same time period. Nevertheless, there were two tests in which the obtained results were no representative due to the difficulties they had to achieve a stability in the measurements with a high thermal gradient, although it could also be attributed to a possible degradation of the thermal performance of these walls. That degradation caused differences between the estimated value from ISO 6946 and the measured value. For these tests, the application of correction could reduce the error with respect to the estimated *U*-value, reducing the deviation percentage from 75% to 59% in W3 and from 90% to 33% in W5, although the result continued being non-representative.

Therefore, in most of the cases analysed, Eq. (4) obtained valid results when the test lasted between 3 and 7 days, whereas for Eqs. (12) and (15) representative values could be obtained on the second day, although it is possible that the use of the method produces non-representative results depending on the test conditions and the previous knowledge of the wall. Regarding the values obtained by Eqs. (12) and (15), differences were not detected between the results obtained by the two approaches. This happened because the correction made by *CCF* to thermal conductivity of the materials had no impact on the thermal mass factors calculated in the different walls. The obtained value of thermal transmittance with correction varied 2% only in some façades from *P3*. Regarding relative uncertainty values obtained in all the methods, adequate results with percentages lower than 14% were obtained.

As mentioned above, determining the composition of the wall as well as its thermal properties is fundamental to apply the correction effectively, particularly the layer of insulating material. In Fig. 5, it is represented the data distribution obtained in a test after applying the correction to a configuration of typical wall in Spain under different suppositions of the insulating materials most used in the buildings of the country, varying the thickness and the location with respect to the air gap. Those insulating materials are: mineral wool (MW), polyurethane (PUR), and extruded polystyrene (XPS), which have different thermal conductivity values, density and specific heat according to what is indicated in the constructive elements catalogue [68]. In addition, the position of the insulation with respect to the air gap did not influence the corrected value of the thermal transmittance obtained at each instance. However, the thickness of the insulation and the kind of material had differences on data distributions. The thickness variations for a same material led to deviations between 6.1% and 7.67%, whereas the determination of the insulation had a lower impact on the corrected *U*-value, with deviations between 0.5% and 2.55% for the different types of materials due to the similarity between the thermal properties of the insulation analysed.

Fig. 5. Box-plots of the *U*-values corrected for different estimations of insulation of a wall. GIE: great insulation in external side of air gap; GII: great insulation in internal side of air gap; IE: insulation in external side of air gap; II: insulation in internal side of air gap.

Using the MLP could estimate the *U*-value with the heat storage effect. Since the use of *CCF* did not give a major adjustment of the *U*-value obtained, the output of the proposed MLPs was Eq. (12). As mentioned above, the efficiency of the MLP models was determined by the statistical parameters of R^2, *MAE* and *RMSE*. Table 5 shows the behaviour of the different MLP models in the training time of 5,000. All the MLP models had an adequate correlation coefficient for structures of 7 or more nodes, with R^2 higher than 0.90. Moreover, error statistical parameters had adequate values. In most of the cases, *MAE* was between 0.056 and 0.091, and *RMSE* was between 0.098 and 0.143. The optimal number of neurons was the one with the lowest *MAE* and *RMSE,* and the highest R^2. From the different models analysed, the optimal architecture was the one with 14 neurons for both MLP1 and MLP2.

Table 5
Behaviour of MLP models in training time of 5,000.

Regarding the better adjustment between MLP1 and MLP2, great differences in the quality parameters of both optimal configurations of networks for 120,000 training cycles were not detected (Fig. 6), although the statistical parameters obtained in MLP1 were more adequate. Carrying out transformations into the input variables did not lead to an improvement in the parameters of the models. MLP1 had values of *MAE* and *RMSE* lower than MLP2, increasing from 0.050 to 0.057 and from 0.081 to 0.092, respectively. Moreover, the R^2 had a better adjustment in MLP1, going from 95.69% to 94.31% for MLP2. Fig. 5 shows how the points cloud for MLP1 had more precise predictions with an error lower than MLP2. Thus, the most correct model was MLP1 with 14 neurons, since the quality parameters were better. Furthermore, carrying out transformations in the input variables were not required, so that the process to estimate the thermal transmittance was simplified.

Fig. 6. Correlation between the predicted value and the expected value in the training cycle 120,000, and statistical parameters obtained for the architectures of 14 nodes of MLP1 and MLP2.

After training the network, three new case studies no included in the training of MLP were tested (see Table 3). Fig. 7 shows the time serie of the *U*-value, and Table 6 shows the results obtained at the end of the test for Eqs. (4) and (12) as well as for the MLP model, for both data without post-processing and with post-processing, rejecting the measurements performed in the first 24 h. For the estimation uncertainty carried out by the MLP, the error associated with the model

prediction was considered as well as the contributions associated with the variation of the type of insulating material and its thickness discussed above (Fig. 5).

Fig. 7. Time series of *U*-value for the different methods: (a) without post-processing; and (b) with post-processing. Eq. (4) is represented by the red line, Eq. (12) is represented by the blue line, and the estimation of the MLP is represented by the black line. The expected value in case studies is represented by the grey dashed line.

Table 6
U-value obtained in the three case studies of testing.

The results obtained by the MLP were adequate in the three typologies of façades, corresponding to *P1*, *P2* and *P3*. The stability in the estimation of thermal transmittance varied according to the the wall typology. In case study B, valid results were obtained on the second day of the measurement, whereas it was necessary to extend the test to 4 days in case study C due to the highest thermal resistance that the wall had and the inestability of the thermal gradient during the test because of the variations of external temperature. In case study A, an improvement in the estimation of *U*-value in comparison with the value obtained for Eqs. (4) and (12) was not detected. The deviation between the expected *U*-value and the one estimated by the MLP was lower than 20% in all the case studies, having a minimum percentage deviation of 2% in case study B. Thus, the MLP was well adapted to the walls from the different considered building periods. It is important to highlight that the MLP did not require to carry out a data processing in order to obtain estimations adjusted to the expected value of thermal transmittance, since thermal variations which took place during the test did not significantly affect the final value estimated by the network, with small reductions of the error percentage of 4.55% in CS-A, 0% in CS-B, and 1.72% in CS-C (see Table 6). So, the use of the MLP could optimize the estimation procedure of thermal transmittance because making the data post-processing was not required.

Although ANNs have been widely used as classification models in scientific literature, ANNs are used in this article as data analysis methodology monitored to assess thermal transmittance.

The data analysis methodology proposed in this paper used eight input variables (T_{in}, T_{out}, $T_{s,in}$, δT_{in}, δT_{out}, s, Δt, P) to determine the thermal transmittance of the walls by using THM with corrections for storage effects (see Fig. 8). From these data, only temperature variables (T_{in}, T_{out} and $T_{s,in}$) should be monitored, whereas variables δT_{in}, δT_{out} and Δt were determined automatically according to the data monitored. Only s and P should be determined for the performance of the procedure, but the easiness of identifying them by means of measuring the thickness of the wall and consulting cadastral data did not make the analysis process difficult. After determining the time series of the different variables, they were entered in the MLP developed, and the U-value with the output variable of the model was obtained.

Fig. 8. Flow-chart of the analysis process of a wall using the MLP.

The data analysis model proposed determined accurately the thermal transmittance of walls with insulation, obtaining accurate results in two days for walls of *P2*, and in four days for walls of *P3*. Although differences with respect to the progressive procedure were not obtained for *P1* as walls from this period do not have a high thermal mass, the use of the data analysis model provided valid results, so it could also be used for these walls with the objective of automating the data analysis process. Moreover, the model did not need to carry out a data post-processing, so the calculation procedure was hastened. Another aspect to highlight is that the same methodology of the MLP developed could be used for characterizing thermal transmittance by using the heat flow meter method with corrections for heat storage, extending its use. One of the limitations of the analysis model is that the wall typology should be adapted to the characteristics existing in each region or country. However, the wall typology analysed in this study (multilayer walls with brick layers and an insulation layer) is a constructive technique very common in several countries, such as Belgium, United Kingdom or Italy, and widely analysed in several researches.

6. Conclusions

A calculation methodology has been proposed to determine thermal transmittance by means of the thermometric method considering the heat storage effect, and an artificial neural network of type multilayer perceptron has been developed to simplify its application. Based on the results obtained, the authors of this paper conclude the following:

- The calculation procedure with heat storage correlations suggested in this study for the thermometric method (Eqs. (12) and (15)) was applied to the case studies included in the training dataset. In most case studies, the

calculation procedure allowed to obtain *U*-values with deviations lower than the average method of thermometric method (Eq. (4)), although there were some case studies where the obtained results were non-representatives.

- Differences were not detected in the *U*-values obtained by Eqs. (12) and (15). Hence, the use of conductivity correction factors in the correction for storage effects did not influence the result obtained.
- In walls with insulation in some of their layers, determining the thickness of this material led to variations between 6.1 and 7.67% of the corrected thermal transmittance, while differences because of the type of the existing material in that layer were between 0.5-7.67% due to the similarity in thermal properties of the main insulating materials commonly used.
- A multilayer perceptron has been developed to estimate the *U*-value with the correction for storage effects in order to avoid the need of knowing the composition of the wall. The input variables obtaining a more optimal model were: (i) the internal air temperature; (ii) the external air temperature; (iii) the internal surface temperature; (iv) the difference of the average internal temperature; (v) the difference of the average external temperature; (vi) the thickness of the wall; (vii) the building period; and (viii) the time interval between the measurements. These input variables could be obtained by means of a methodology of monitoring the simple wall which can be applied to any energy audit. The multilayer perceptron model with an optimal behaviour was the one of 14 nodes in the hidden layer and without carrying out transformations in the input variables, with a R^2 of 0.957, a *MAE* of 0.050, and a *RMSE* of 0.081.
- The multilayer perceptron obtained valid results in the testing for the three considered building periods (*P1*, *P2,* and *P3*), with deviations lower than 20% between the measured value and the expected value, and varying the test duration according to the thermal resistance of the wall and the variations of external temperature. In this sense, valid results were obtained in two days in *P2*, while it was necessary to extend the test to 4 days in *P3*. Thus, the data analysis model proposed leads to obtain valid results in time periods shorter than those recommended by several researches.
- The multilayer perceptron did not need a data post-processing to obtain representative results, optimizing the speed of the calculation procedure, although the post-processing reduced the error percentage up to 4.55%.

To conclude, the multilayer perceptron developed in this paper can be used for performing energy audits in order to estimate thermal transmittance precisely by applying the thermometric method with correction for storage effects, simplifying and hastening the calculation.

Acknowledgements

This study has been financed by "V Own Research Plan" University of Seville. Authors would like to acknowledge the Agency for Housing and Rehabilitation in Andalusia (AVRA) of the Regional Government of Andalusia for making possible the access to data from their experimental campaigns.

References

[1] WWF, Living Planet Report 2014: Species and spaces, people and places, WWF International, Gland, Switzerland, 2014. doi:10.1007/s13398-014-0173-7.2.

[2] European Commission, A Roadmap for moving to a competitive low carbon economy in 2050, Brussels, Belgium, 2011.

[3] European Environment Agency, Final energy consumption by sector and fuel (2017), Copenhagen, Denmark, 2017. http://www.eea.europa.eu/data-and-maps/indicators/final-energy-consumption-by-sector-9/assessment-1 (accessed March 9, 2017).

[4] Institute for the Energy Diversification and Saving, Balance of the final energy consumption in year 2015 (in Spain), Madrid, Spain, 2016. http://sieeweb.idae.es/consumofinal/bal.asp?txt=2015&tipbal=t (accessed June 1, 2017).

[5] U. Berardi, Clarifying the new interpretations of the concept of sustainable building, Sustain. Cities Soc. 8 (2013) 72–78. doi:10.1016/j.scs.2013.01.008.

[6] S. Ferrari, V. Zanotto, The thermal performance of walls under actual service conditions: Evaluating the results of climatic chamber tests, Constr. Build. Mater. 43 (2013) 309–316. doi:10.1016/j.conbuildmat.2013.02.056.

[7] F. Kurtz, M. Monzón, B. López-Mesa, Energy and acoustics related obsolescence of social housing of Spain's post-war in less favoured urban areas. The case of Zaragoza, Inf. La Construcción. 67 (2015) m021. doi:10.3989/ic.14.062.

[8] J.J. Moyano Campos, D. Antón García, F. Rico Delgado, D. Marín García, Threshold Values for Energy Loss in Building Façades Using Infrared Thermography, in: Sustain. Dev. Renov. Archit. Urban. Eng., Springer International Publishing, 2017: pp. 427–

437. doi:10.1007/978-3-319-51442-0_35.

[9] International Organization for Standardization, ISO 6946:2007 - Building components and building elements - Thermal resistance and thermal transmittance - Calculation method, Geneva, Switzerland, 2007.

[10] G. Desogus, S. Mura, R. Ricciu, Comparing different approaches to in situ measurement of building components thermal resistance, Energy Build. 43 (2011) 2613–2620. doi:10.1016/j.enbuild.2011.05.025.

[11] I. Ballarini, S.P. Corgnati, V. Corrado, Use of reference buildings to assess the energy saving potentials of the residential building stock: The experience of TABULA project, Energy Policy. 68 (2014) 273–284. doi:10.1016/j.enpol.2014.01.027.

[12] International Organization for Standardization, ISO 9869-1:2014 - Thermal insulation - Building elements - In situ measurement of thermal resistance and thermal transmittance. Part 1: Heat flow meter method, Geneva, Switzerland, 2014.

[13] I. Nardi, D. Paoletti, D. Ambrosini, T. De Rubeis, S. Sfarra, U-value assessment by infrared thermography: A comparison of different calculation methods in a Guarded Hot Box, Energy Build. 122 (2016) 211–221. doi:10.1016/j.enbuild.2016.04.017.

[14] J.M. Andújar Márquez, M.Á. Martínez Bohórquez, S. Gómez Melgar, A new metre for cheap, quick, reliable and simple thermal transmittance (U-Value) measurements in buildings, Sensors. 17 (2017) 1–18. doi:10.3390/s17092017.

[15] D. Bienvenido-Huertas, R. Rodríguez-Álvaro, J.J. Moyano, F. Rico, D. Marín, Determining the U-Value of Façades Using the Thermometric Method: Potentials and Limitations, Energies. 11 (2018) 1–17. doi:10.3390/en11020360.

[16] S.-H. Kim, J.-H. Kim, H.-G. Jeong, K.-D. Song, Reliability Field Test of the Air–Surface Temperature Ratio Method for In Situ Measurement of U-Values, Energies. 11 (2018) 1–15. doi:10.3390/en11040803.

[17] X. Meng, B. Yan, Y. Gao, J. Wang, W. Zhang, E. Long, Factors affecting the in situ measurement accuracy of the wall heat transfer coefficient using the heat flow meter method, Energy Build. 86 (2015) 754–765. doi:10.1016/j.enbuild.2014.11.005.

[18] H. Trethowen, Measurement errors with surface-mounted heat flux sensors, Build. Environ. 21 (1986) 41–56. doi:10.1016/0360-1323(86)90007-7.

[19] R. Albatici, A.M. Tonelli, M. Chiogna, A comprehensive experimental approach for the validation of quantitative infrared thermography in the evaluation of building thermal transmittance, Appl. Energy. 141 (2015) 218–228. doi:10.1016/j.apenergy.2014.12.035.

[20] K.E.A. Ohlsson, T. Olofsson, Quantitative infrared thermography imaging of the density of heat flow rate through a building element surface, Appl. Energy. 134 (2014) 499–505. doi:10.1016/j.apenergy.2014.08.058.

[21] P.A. Fokaides, S.A. Kalogirou, Application of infrared thermography for the determination of the overall heat transfer coefficient (U-Value) in building envelopes, Appl. Energy. 88 (2011) 4358–4365. doi:10.1016/j.apenergy.2011.05.014.

[22] A. Reilly, O. Kinnane, The impact of thermal mass on building energy consumption, Appl. Energy. 198 (2017) 108–121. doi:10.1016/j.apenergy.2017.04.024.

[23] S.A. Al-Sanea, M.F. Zedan, Improving thermal performance of building walls by optimizing insulation layer distribution and thickness for same thermal mass, Appl. Energy. 88 (2011) 3113–3124. doi:10.1016/j.apenergy.2011.02.036.

[24] G. Dall'O', L. Sarto, A. Panza, Infrared screening of residential buildings for energy audit purposes: Results of a field test, Energies. 6 (2013) 3859–3878. doi:10.3390/en6083859.

[25] A.H. Deconinck, S. Roels, Comparison of characterisation methods determining the thermal resistance of building components from onsite measurements, Energy Build. 130 (2016) 309–320. doi:10.1016/j.enbuild.2016.08.061.

[26] E. Genova, G. Fatta, The thermal performances of historic masonry: In-situ measurements of thermal conductance on calcarenite stone walls in Palermo, Energy Build. 168 (2018) 363–373. doi:10.1016/j.enbuild.2018.03.009.

[27] F. Asdrubali, F. D'Alessandro, G. Baldinelli, F. Bianchi, Evaluating in situ thermal transmittance of green buildings masonries: A case study, Case Stud. Constr. Mater. 1 (2014) 53–59. doi:10.1016/j.cscm.2014.04.004.

[28] I. Nardi, D. Ambrosini, T. De Rubeis, S. Sfarra, S. Perilli, G. Pasqualoni, A comparison between thermographic and flow-meter methods for the evaluation of thermal transmittance of different wall constructions, J. Phys. Conf. Ser. 655 (2015) 1–10. doi:10.1088/1742-6596/655/1/012007.

[29] T. Samardzioska, R. Apostolska, Measurement of heat-flux of new type façade walls, Sustainability. 8 (2016) 1–11. doi:10.3390/su8101031.

[30] K. Gaspar, M. Casals, M. Gangolells, Energy & Buildings In situ measurement of façades with a low U-value : Avoiding deviations, Energy Build. 170 (2018) 61–73. doi:10.1016/j.enbuild.2018.04.012.

[31] A. Rasooli, L. Itard, C.I. Ferreira, A response factor-based method for the rapid in-situ determination of wall's thermal resistance

in existing buildings, Energy Build. 119 (2016) 51–61. doi:10.1016/j.enbuild.2016.03.009.

[32] G. Ficco, F. Iannetta, E. Ianniello, F.R. D'Ambrosio Alfano, M. Dell'Isola, U-value in situ measurement for energy diagnosis of existing buildings, Energy Build. 104 (2015) 108–121. doi:10.1016/j.enbuild.2015.06.071.

[33] Energy Saving Trust, CE128/GIR64: Post-construction testing – a professionals guide to testing housing for energy efficiency, 2005.

[34] I. Naveros, M.J. Jiménez, M.R. Heras, Analysis of capabilities and limitations of the regression method based in averages, applied to the estimation of the U value of building component tested in Mediterranean weather, Energy Build. 55 (2012) 854–872. doi:10.1016/j.enbuild.2012.09.028.

[35] S.-H. Kim, J.-H. Lee, J.-H. Kim, S.-H. Yoo, H.-G. Jeong, The Feasibility of Improving the Accuracy of In Situ Measurements in the Air-Surface Temperature Ratio Method, Energies. 11 (2018) 1–18. doi:10.3390/en11071885.

[36] P.G. Cesaratto, M. De Carli, A measuring campaign of thermal conductance in situ and possible impacts on net energy demand in buildings, Energy Build. 59 (2013) 29–36. doi:10.1016/j.enbuild.2012.08.036.

[37] D.S. Choi, M.J. Ko, Comparison of Various Analysis Methods Based on Heat Flowmeters and Infrared Thermography Measurements for the Evaluation of the In Situ Thermal Transmittance of Opaque Exterior Walls, Energies. 10 (2017) 1–22. doi:10.3390/en10071019.

[38] R. Pino-Mejías, A. Pérez-Fargallo, C. Rubio-Bellido, J.A. Pulido-Arcas, Comparison of linear regression and artificial neural networks models to predict heating and cooling energy demand, energy consumption and CO2 emissions, Energy. 118 (2017) 24–36. doi:10.1016/j.energy.2016.12.022.

[39] S.A. Kalogirou, Applications of artificial neural-networks for energy systems, Appl. Energy. 67 (2000) 17–35. doi:10.1016/S0306-2619(00)00005-2.

[40] R. Kumar, R.K. Aggarwal, J.D. Sharma, Energy analysis of a building using artificial neural network: A review, Energy Build. 65 (2013) 352–358. doi:10.1016/j.enbuild.2013.06.007.

[41] A. Kialashaki, J.R. Reisel, Modeling of the energy demand of the residential sector in the United States using regression models and artificial neural networks, Appl. Energy. 108 (2013) 271–280. doi:10.1016/j.apenergy.2013.03.034.

[42] S. Chudzik, Applying infrared measurements in a measuring system for determining thermal parameters of thermal insulation materials, Infrared Phys. Technol. 81 (2017) 296–304. doi:10.1016/j.infrared.2016.12.025.

[43] C. Buratti, L. Barelli, E. Moretti, Application of artificial neural network to predict thermal transmittance of wooden windows, Appl. Energy. 98 (2012) 425–432. doi:10.1016/j.apenergy.2012.04.004.

[44] S.S. Sablani, A. Kacimov, J. Perret, A.S. Mujumdar, A. Campo, Non-iterative estimation of heat transfer coefficients using artificial neural network models, Int. J. Heat Mass Transf. 48 (2005) 665–679. doi:10.1016/j.ijheatmasstransfer.2004.09.005.

[45] R. Singh, R.S. Bhoopal, S. Kumar, Prediction of effective thermal conductivity of moist porous materials using artificial neural network approach, Build. Environ. 46 (2011) 2603–2608. doi:10.1016/j.buildenv.2011.06.019.

[46] A. Mitra, A. Majumdar, P.K. Majumdar, D. Bannerjee, Predicting thermal resistance of cotton fabrics by artificial neural network model, Exp. Therm. Fluid Sci. 50 (2013) 172–177. doi:10.1016/j.expthermflusci.2013.06.006.

[47] L. Evangelisti, C. Guattari, P. Gori, R. de Lieto Vollaro, F. Asdrubali, Experimental investigation of the influence of convective and radiative heat transfers on thermal transmittance measurements, Int. Commun. Heat Mass Transf. 78 (2016) 214–223. doi:10.1016/j.icheatmasstransfer.2016.09.008.

[48] W. Wild, Application of infrared thermography in civil engineering, Proc. Est. Acad. Sci. Eng. 13 (2007) 436–444.

[49] L. Peeters, I. Beausoleil-Morrison, A. Novoselac, Internal convective heat transfer modeling: Critical review and discussion of experimentally derived correlations, Energy Build. 43 (2011) 2227–2239. doi:10.1016/j.enbuild.2011.05.002.

[50] A.J.N. Khalifa, R.H. Marshall, Validation of heat transfer coefficients on interior building surfaces using a real-sized indoor test cell, Int. J. Heat Mass Transf. 33 (1990) 2219–2236. doi:10.1016/0017-9310(90)90122-B.

[51] L. Evangelisti, C. Guattari, F. Asdrubali, Influence of heating systems on thermal transmittance evaluations: Simulations, experimental measurements and data post-processing, Energy Build. 168 (2018) 180–190. doi:10.1016/j.enbuild.2018.03.032.

[52] V. Echarri, A. Espinosa, C. Rizo, Thermal transmission through existing building enclosures: Destructive monitoring in intermediate layers versus non-destructive monitoring with sensors on surfaces, Sensors. 17 (2017) 1–24. doi:10.3390/s17122848.

[53] F. Domínguez-Muñoz, B. Anderson, J.M. Cejudo-López, A. Carrillo-Andrés, Uncertainty in the thermal conductivity of insulation materials, Energy Build. 42 (2010) 2159–2168. doi:10.1016/j.enbuild.2010.07.006.

[54] International Organization for Standardization, ISO 10456:2007 - Building materials and products - Hygrothermal properties - Tabulated design values and procedures for determining declared and design thermal values, Geneva, Switzerland, 2007.

[55] J.M. Pérez-Bella, J. Domínguez-Hernández, E. Cano-Suñén, J.J. Del Coz-Díaz, F.P. Álvarez Rabanal, A correction factor to approximate the design thermal conductivity of building materials. Application to Spanish façades, Energy Build. 88 (2015) 153–164. doi:10.1016/j.enbuild.2014.12.005.

[56] P. Gaurang, G. Amit, Y. Kosta, P. Devyani, Behaviour Analysis of Multilayer Perceptrons with Multiple Hidden Neurons and Hidden Layers, Int. J. Comput. Theory Eng. 3 (2011) 332–337.

[57] M. Gangolells, M. Casals, N. Forcada, M. MacArulla, E. Cuerva, Energy mapping of existing building stock in Spain, J. Clean. Prod. 112 (2016) 3895–3904. doi:10.1016/j.jclepro.2015.05.105.

[58] The Government of Spain, Royal Decree 2429/79. Approving the Basic Building Norm NBE-CT-79, about the Thermal Conditions in Buildings, 1979.

[59] The Government of Spain, Royal Decree 314/2006. Approving the Spanish Technical Building Code CTE-DB-HE-1, Madrid, Spain, 2013.

[60] V.F. Membrive, L.B. Xavier, F.P. Isabel, Clasificación energética de edificios. Efectos del cambio en la normativa y los métodos constructivos en la zona climática española A4, Obs. Medioambient. 16 (2013) 69–98.

[61] D.E. Rumelhart, G.E. Hinton, R.J. Williams, Learning representations by back-propagating errors, Nature. 323 (1986) 533–536. doi:10.1038/323533a0.

[62] R. Fletcher, Practical methods of optimization, John Wiley&Sons, Chichester - New York - Brisbane - Toronto, United States, 1980.

[63] A. Golbabai, S. Seifollahi, Radial basis function networks in the numerical solution of linear integro-differential equations, Appl. Math. Comput. 188 (2007) 427–432. doi:10.1016/j.amc.2006.10.004.

[64] A. Alimissis, K. Philippopoulos, C.G. Tzanis, D. Deligiorgi, Spatial estimation of urban air pollution with the use of artificial neural network models, Atmos. Environ. (2018). doi:10.1016/j.atmosenv.2018.07.058.

[65] M.K. Singh, S. Mahapatra, J. Teller, An analysis on energy efficiency initiatives in the building stock of Liege, Belgium, Energy Policy. 62 (2013) 729–741. doi:10.1016/j.enpol.2013.07.138.

[66] P. Baker, U-values and traditional buildings: in situ measurements and their comparisons to calculated values, 2011.

[67] S.P. Corgnati, E. Fabrizio, M. Filippi, V. Monetti, Reference buildings for cost optimal analysis: Method of definition and application, Appl. Energy. 102 (2013) 983–993. doi:10.1016/j.apenergy.2012.06.001.

[68] Eduardo Torroja Institute for Construction Science, Constructive elements catalogue of the CTE, 2010.

[69] International Organization for Standardization, ISO/IEC Guide 98-3:2008 - Uncertainty of measurement - Part 3: Guide to the expression of uncertainty in measurement (GUM:1995), Geneva, Switzerland, 2008.

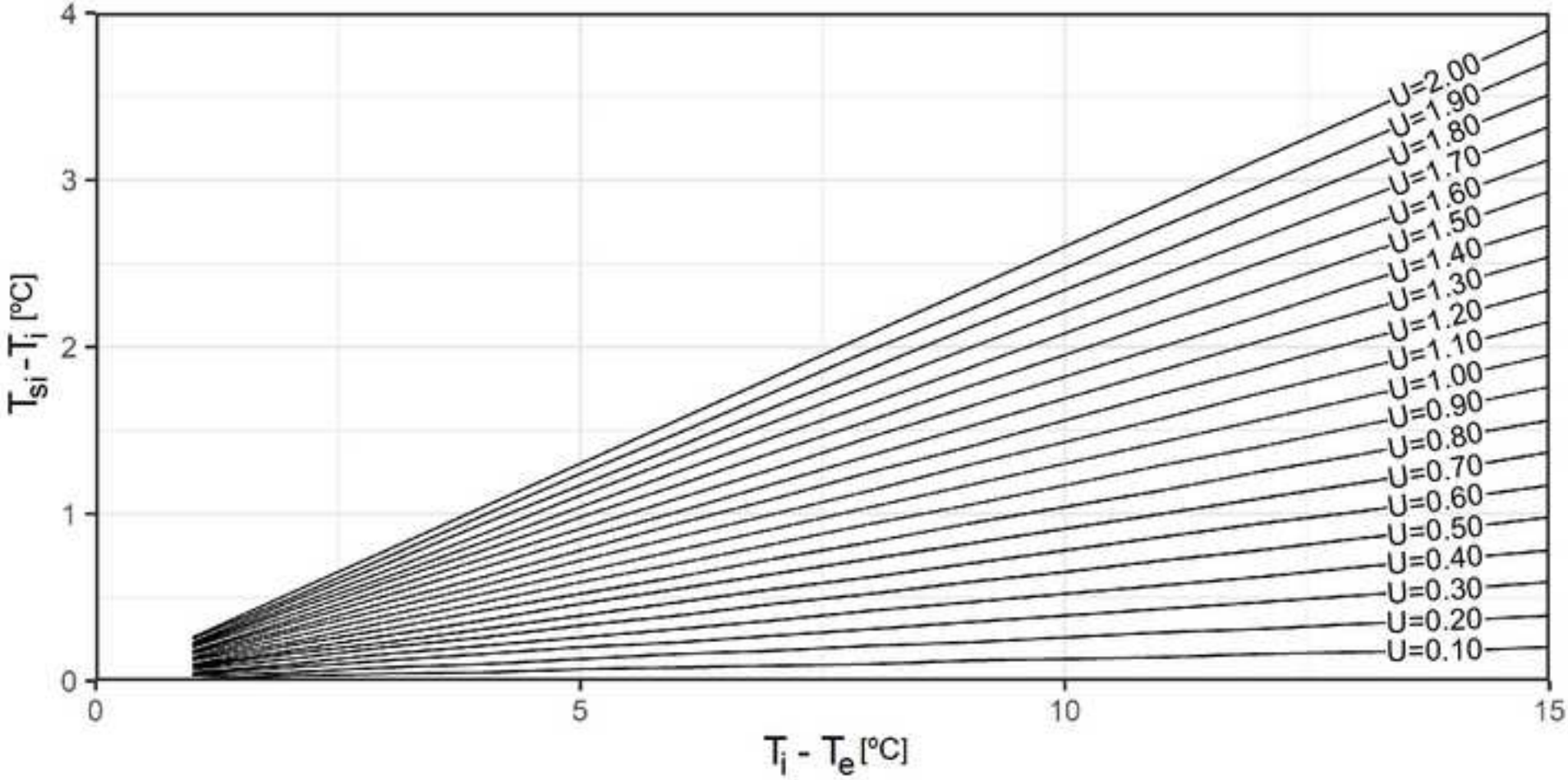
4
3
2
1
0
0
5
10
15
T_{si} - T_i [ºC]
T_i - T_e [ºC]
U=2.00
U=1.90
U=1.80
U=1.70
U=1.60
U=1.50
U=1.40
U=1.30
U=1.20
U=1.10
U=1.00
U=0.90
U=0.80
U=0.70
U=0.60
U=0.50
U=0.40
U=0.30
U=0.20
U=0.10

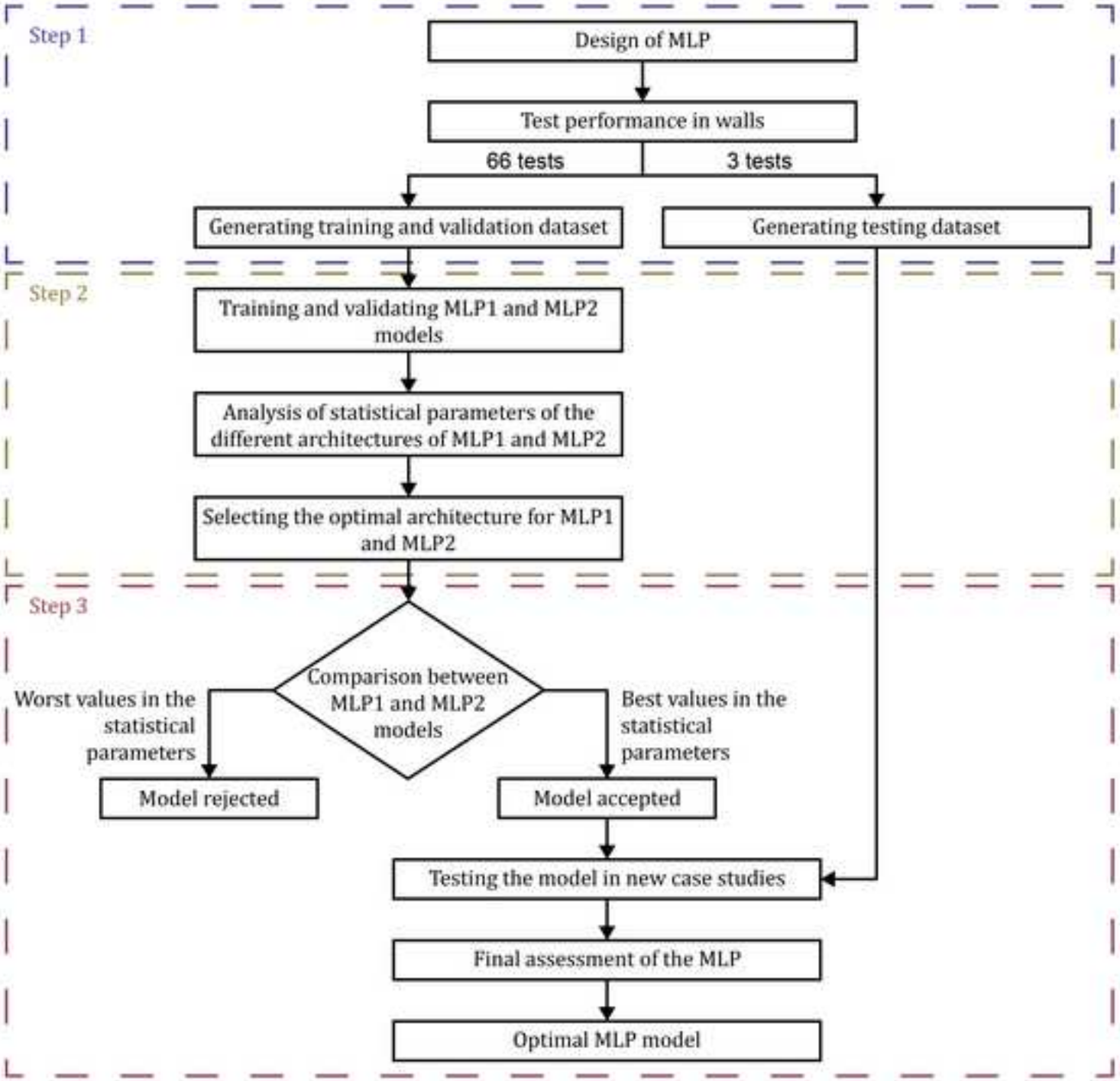
Step 1
Design of MLP
Test performance in walls
66 tests
3 tests
Generating training and validation dataset
Generating testing dataset
Step 2
Training and validating MLP1 and MLP2 models
Analysis of statistical parameters of the different architectures of MLP1 and MLP2
Selecting the optimal architecture for MLP1 and MLP2
Step 3
Comparison between MLP1 and MLP2 models
Worst values in the statistical parameters
Best values in the statistical parameters
Model rejected
Model accepted
Testing the model in new case studies
Final assessment of the MLP
Optimal MLP model

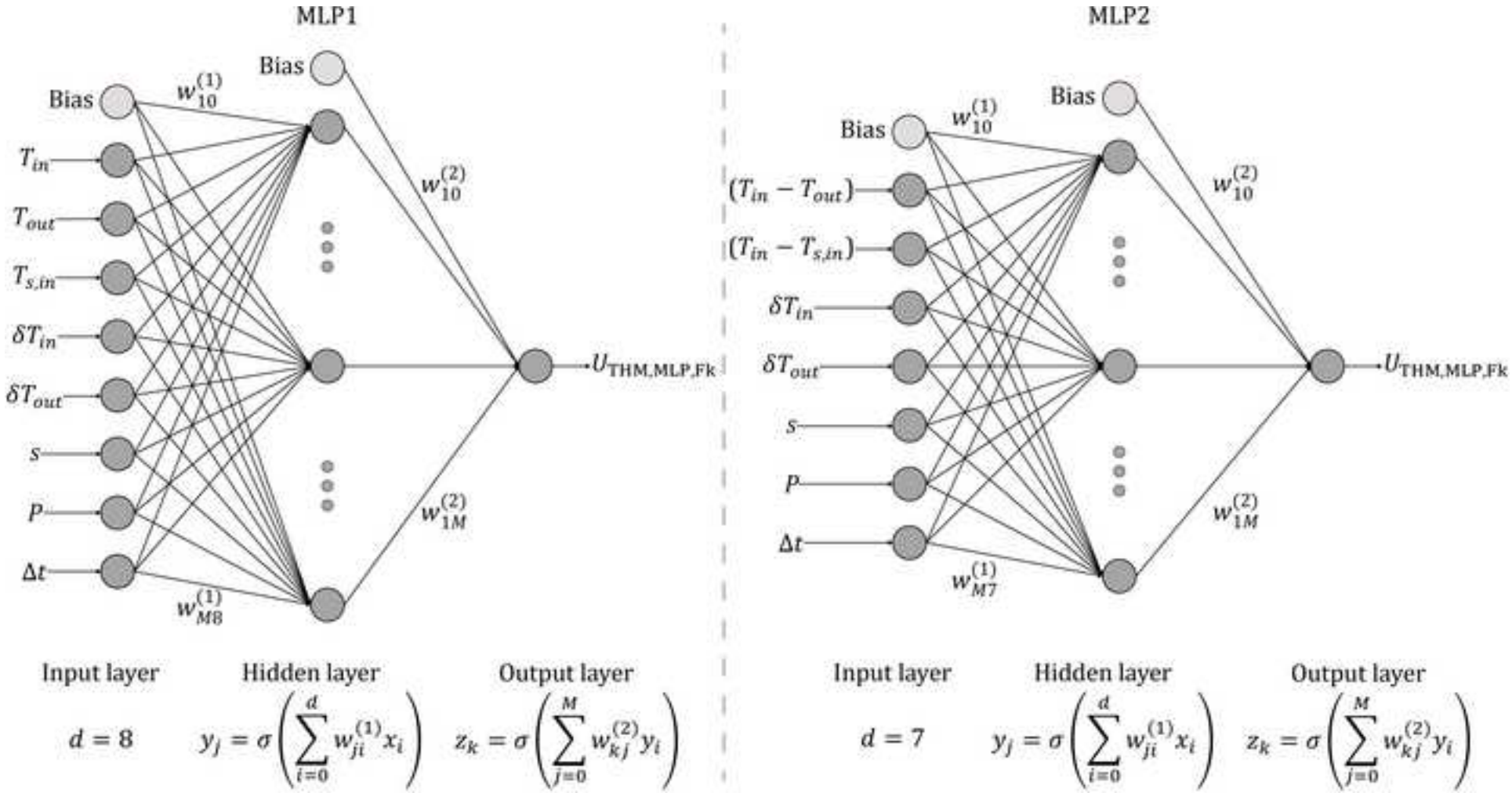

Input layer | Hidden layer | Output layer

$d = 8$ $\quad y_j = \sigma\left(\sum_{i=0}^{d} w_{ji}^{(1)} x_i\right) \quad z_k = \sigma\left(\sum_{j=0}^{M} w_{kj}^{(2)} y_i\right)$

Input layer | Hidden layer | Output layer

$d = 7$ $\quad y_j = \sigma\left(\sum_{i=0}^{d} w_{ji}^{(1)} x_i\right) \quad z_k = \sigma\left(\sum_{j=0}^{M} w_{kj}^{(2)} y_i\right)$

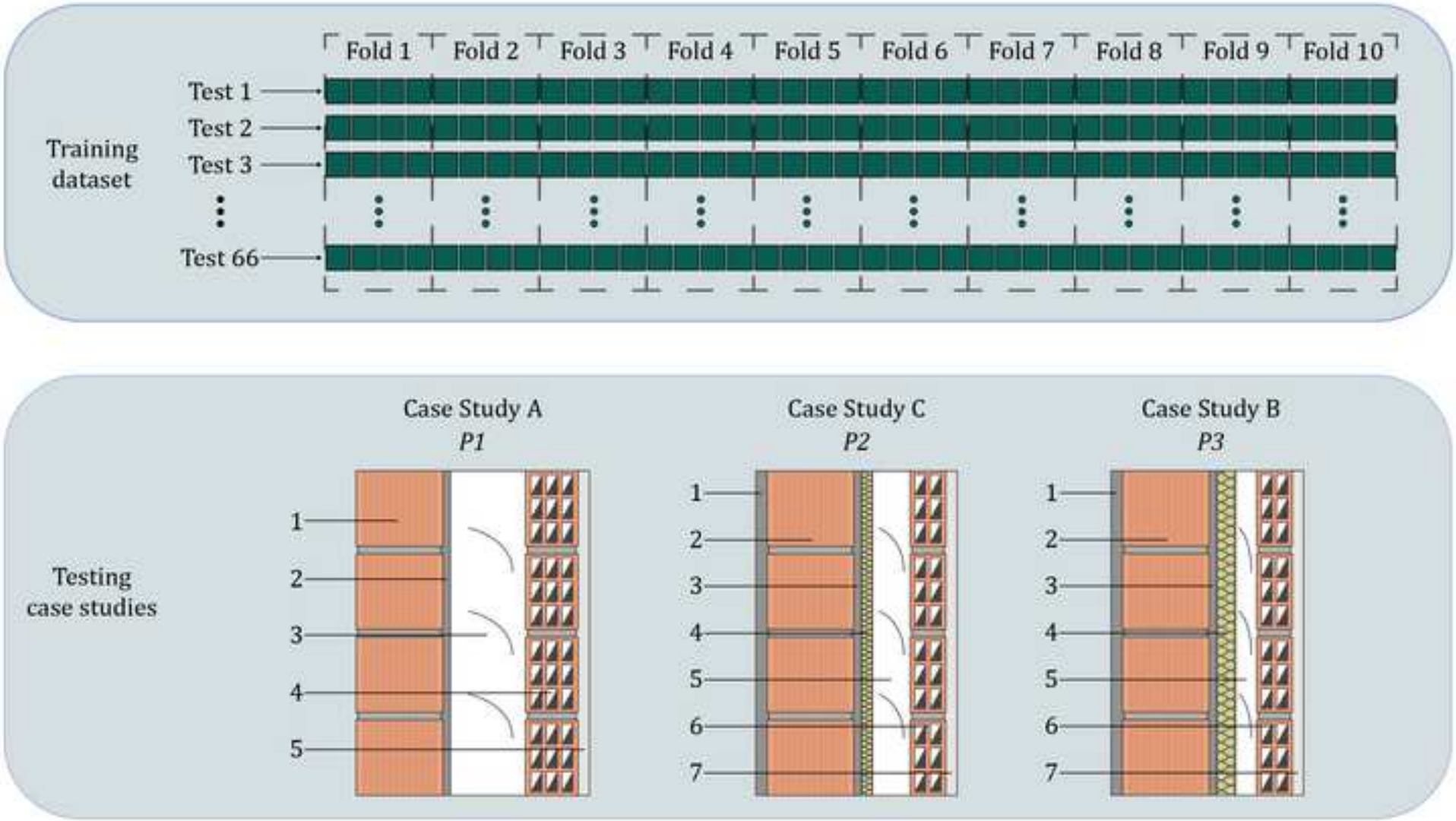
Training dataset
Fold 1
Fold 2
Fold 3
Fold 4
Fold 5
Fold 6
Fold 7
Fold 8
Fold 9
Fold 10
Test 1
Test 2
Test 3
Test 66
Testing case studies
Case Study A
P1
Case Study C
P2
Case Study B
P3
1
2
3
4
5
6
7

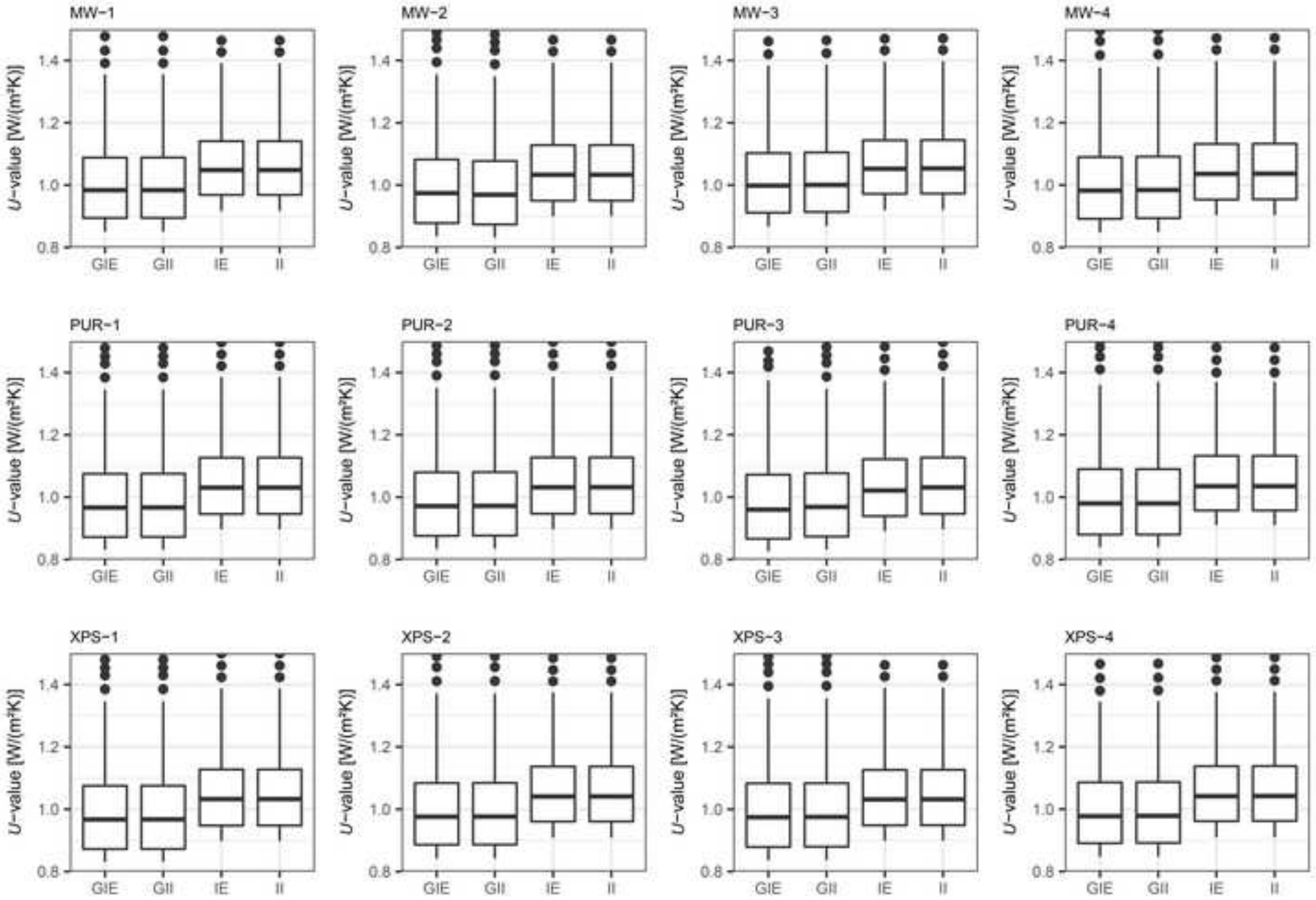
MW-1
MW-2
MW-3
MW-4
PUR-1
PUR-2
PUR-3
PUR-4
XPS-1
XPS-2
XPS-3
XPS-4
U-value [W/(m²K)]
0.8
1.0
1.2
1.4
GIE
GII
IE
II

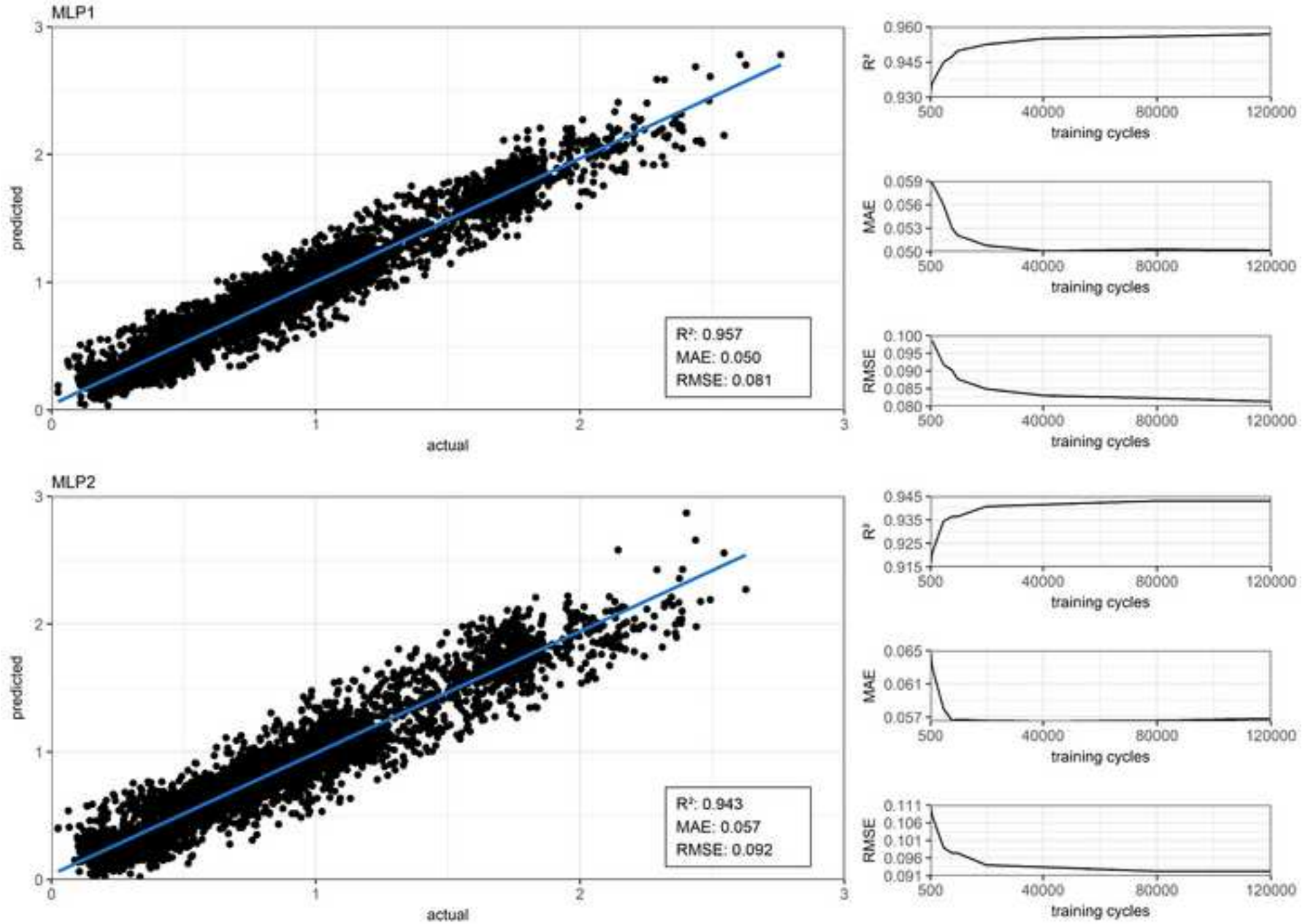
MLP1
predicted
actual
R²: 0.957
MAE: 0.050
RMSE: 0.081
R²
MAE
RMSE
training cycles
MLP2
predicted
actual
R²: 0.943
MAE: 0.057
RMSE: 0.092
R²
MAE
RMSE
training cycles

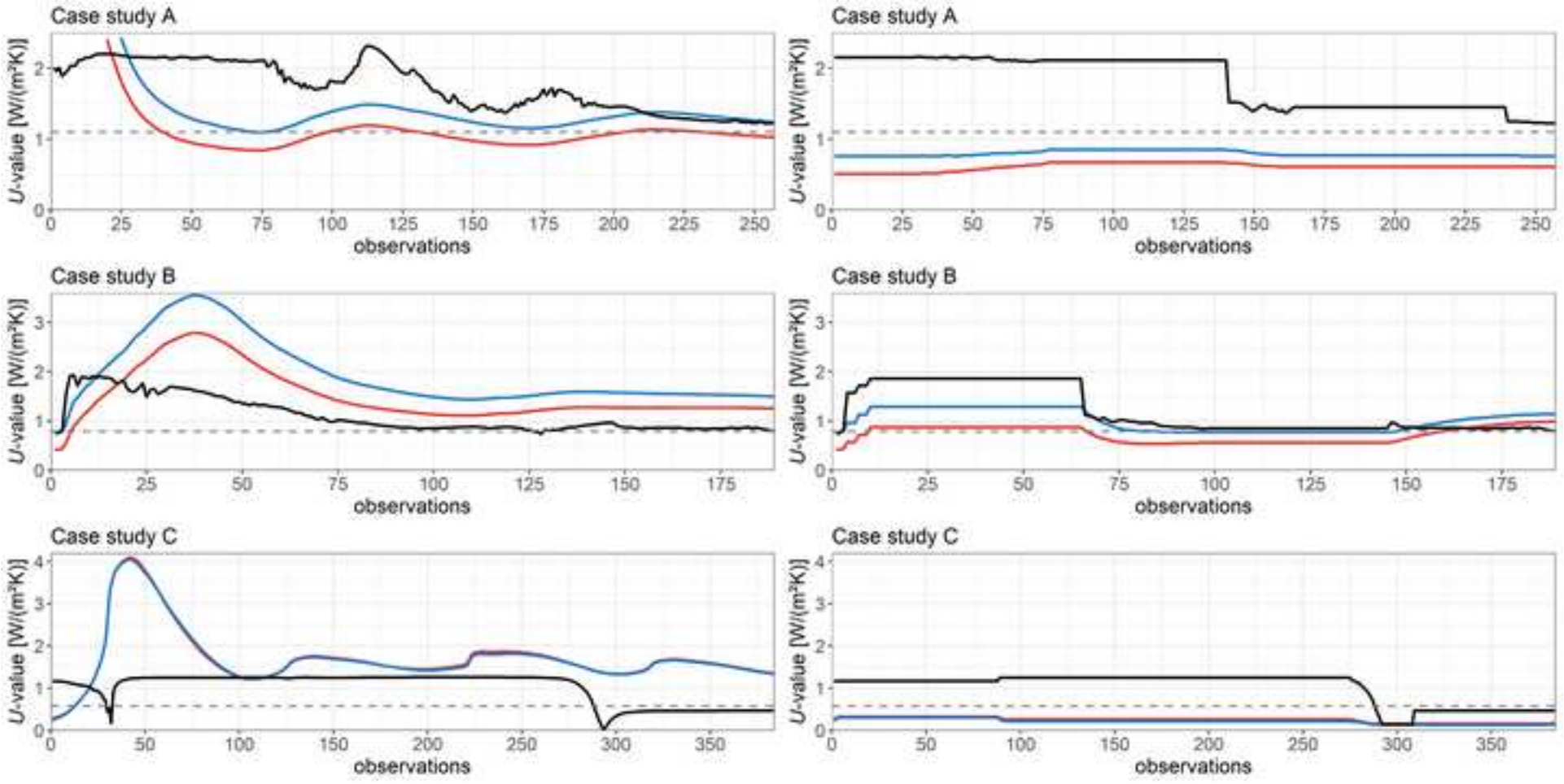
Case study A
U-value [W/(m²K)]
observations
Case study B
U-value [W/(m²K)]
observations
Case study C
U-value [W/(m²K)]
observations
Case study A
U-value [W/(m²K)]
observations
Case study B
U-value [W/(m²K)]
observations
Case study C
U-value [W/(m²K)]
observations

(a) (b)

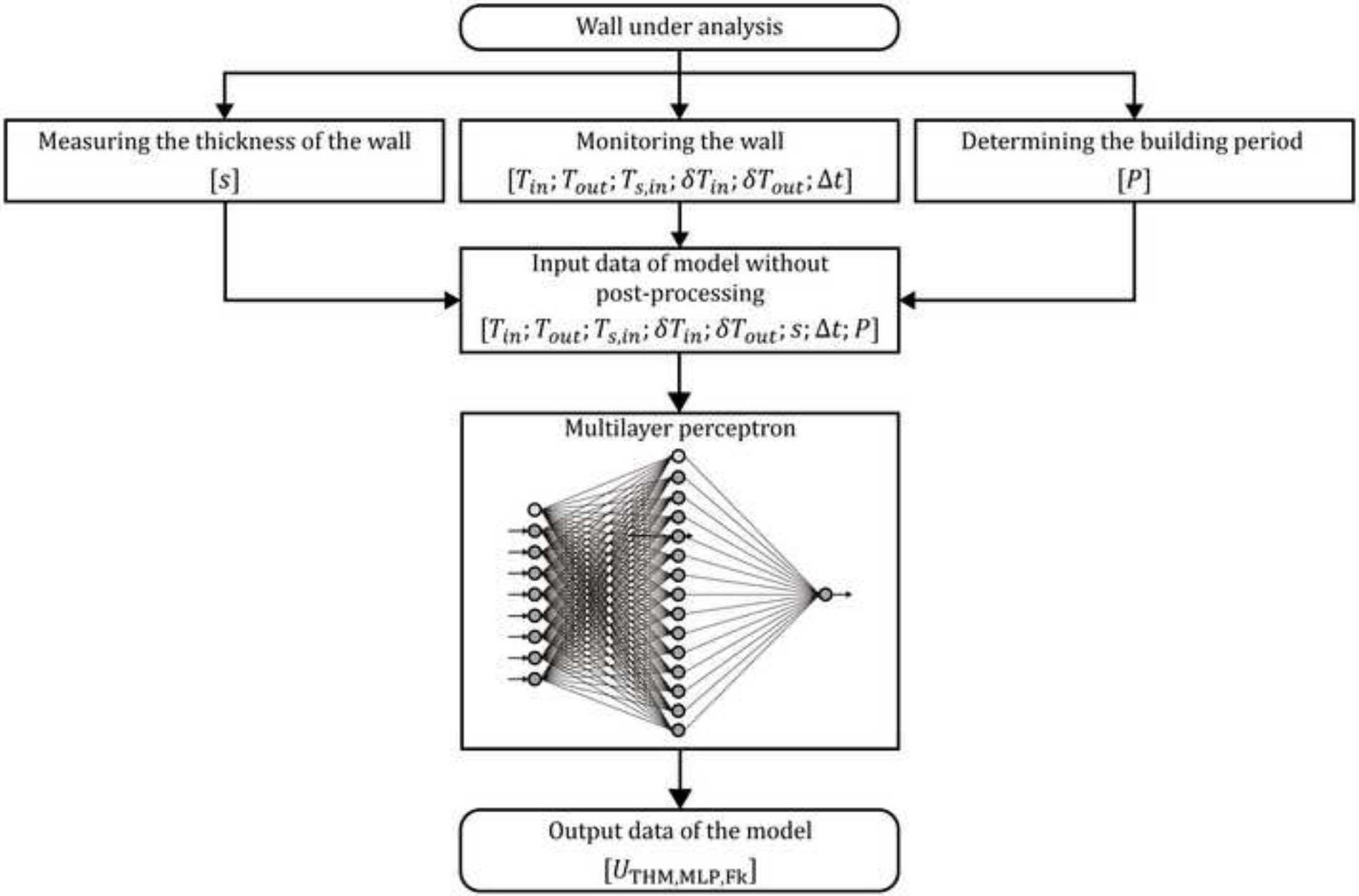
Wall under analysis
Measuring the thickness of the wall
[s]
Monitoring the wall
[T_in; T_out; T_s,in; δT_in; δT_out; Δt]
Determining the building period
[P]
Input data of model without post-processing
[T_in; T_out; T_s,in; δT_in; δT_out; s; Δt; P]
Multilayer perceptron
Output data of the model
[U_THM,MLP,Fk]

Table 1
CCF for the locations of the analysed walls.

Location	*CCF* [a]
Cadiz	1.0403
Cordoba	1.0367
Granada	1.0311
Huelva	1.0385
Jaen	1.0354
Malaga	1.0382
Seville	1.0385

[a] Conductivity correction factor given by Pérez-Bella et al. [33].

Table 2
Input and output data compiled in datasets for both models of MLP.

Model	Input data	Class
MLP1	$[T_{in}; T_{out}; T_{s,in}; \delta T_{in}; \delta T_{out}; s; \Delta t; P]$	$U_{\mathrm{THM,MLP,Fk}}$
MLP2	$[T_{in} - T_{out}; T_{in} - T_{s,in}; \delta T_{in}; \delta T_{out}; s; \Delta t; P]$	$U_{\mathrm{THM,MLP,Fk}}$

Table 3
Technical characteristics and thermophysical properties of the walls used for testing the MLP.

#	Case Study A *P1* (before NBE-CT-79)	s [mm]	c_p [J/(kg·K)]	ρ [kg/m³]	λ [W/(m·K)]	R [(m²·K)/W]
1	Perforated brick	115	1000	780	0.35	-
2	Cement mortar	10	1000	1900	1.30	-
3	Air gap	100	-	-	-	0.18
4	Hollow brick	70	1000	770	0.32	-
5	Gypsum plaster	15	1000	1000	0.57	-
$R_{s,in}$=0.13 [(m²·K)/W]						
$R_{s,out}$=0.04 [(m²·K)/W]						
CCF=1.0385 [a] [dimensionless]						
U = 1.10 [W/(m²·K)] [b]						
#	Case Study B *P2* (between NBE-CT-79 and CTE)	s [mm]	c_p [J/(kg·K)]	ρ [kg/m³]	λ [W/(m·K)]	R [(m²·K)/W]
1	Cement mortar	15	1000	1900	1.30	-
2	Perforated brick	115	1000	780	0.35	-
3	Cement mortar	10	1000	1900	1.30	-
4	Insulation PUR	15	1400	40	0.035	-
5	Air gap	50	-	-	-	0.18
6	Hollow brick	50	1000	770	0.32	-
7	Gypsum plaster	15	1000	1000	0.57	-
$R_{s,in}$=0.13 [(m²·K)/W]						
$R_{s,out}$=0.04 [(m²·K)/W]						
CCF=1.0385 [a] [dimensionless]						
U = 0.79 [W/(m²·K)] [b]						
#	Case Study C *P3* (after CTE)	s [mm]	c_p [J/(kg·K)]	ρ [kg/m³]	λ [W/(m·K)]	R [(m²·K)/W]
1	Cement mortar	15	1000	1900	1.30	-
2	Perforated brick	117	1000	780	0.35	-
3	Cement mortar	10	1000	1900	1.30	-
4	Insulation PUR	25	1400	35	0.028	-
5	Air gap	28	-	-	-	0.18
6	Hollow brick	50	1000	770	0.32	-
7	Gypsum plaster	15	1000	1000	0.57	-
$R_{s,in}$=0.13 [(m²·K)/W]						
$R_{s,out}$=0.04 [(m²·K)/W]						
CCF=1.0385 [a] [dimensionless]						
U = 0.58 [W/(m²·K)] [b]						

s: thickness; c_p: specific heat capacity; ρ: density; λ: thermal conductivity; R: thermal resistance.

[a] Conductivity correction factor given by Pérez-Bella et al. [33].

[b] U-value estimated according to the calculation procedure from ISO 6946 [27].

Table 4
Results obtained for some of the walls of the training dataset.

Wall	Period	$U_{\text{Estimated}}$ [a]	U_{THM} [b] (2 days)	U_{THM} [b] (3 days)	$U_{\text{THM,Fk}}$ [c] (2 days)	$U_{\text{THM,Fk}}$ [c] (3 days)	$U_{\text{THM,Fk,CCF}}$ [d] (2 days)	$U_{\text{THM,Fk,CCF}}$ [d] (3 days)
W1	*P1*	1.09	0.86 ± 0.09	0.91 ± 0.07	1.01 ± 0.11	1.05 ± 0.07	1.01 ± 0.11	1.05 ± 0.07
W2	*P1*	1.60	1.22 ± 0.08	1.31 ± 0.07	1.75 ± 0.18	1.74 ± 0.13	1.75 ± 0.18	1.74 ± 0.13
W3	*P2*	0.81	1.42 ± 0.08	1.27 ± 0.05	1.29 ± 0.07	1.28 ± 0.05	1.29 ± 0.07	1.28 ± 0.05
W4	*P2*	0.85	0.65 ± 0.07	0.83 ± 0.07	0.96 ± 0.11	1.07 ± 0.10	0.96 ± 0.11	1.07 ± 0.10
W5	*P3*	0.61	1.67 ± 0.11	1.16 ± 0.10	1.41 ± 0.10	0.81 ± 0.08	1.41 ± 0.10	0.80 ± 0.08
W6	*P3*	0.76	0.80 ± 0.08	0.86 ± 0.06	0.73 ± 0.09	0.75 ± 0.10	0.73 ± 0.09	0.75 ± 0.10

[a] Estimated *U*-value according to the calculation procedure from ISO 6946 [27].
[b] *U*-value obtained from Eq. (4).
[c] *U*-value obtained from Eq. (12).
[d] *U*-value obtained from Eq. (15).

Table 5
Behaviour of the MLP models in training time of 5,000.

MLP	Indicators	Number of nodes in the hidden layer											
		4	5	6	7	8	9	10	11	12	13	14	15
MLP1	R^2	0.863	0.877	0.893	0.904	0.914	0.927	0.929	0.931	0.932	0.934	0.936	0.934
	MAE	0.083	0.082	0.075	0.073	0.07	0.059	0.060	0.056	0.060	0.060	0.058	0.056
	RMSE	0.142	0.134	0.126	0.119	0.113	0.105	0.102	0.098	0.100	0.099	0.098	0.098
MLP2	R^2	0.862	0.894	0.895	0.912	0.908	0.904	0.913	0.917	0.918	0.920	0.921	0.918
	MAE	0.091	0.081	0.075	0.071	0.069	0.069	0.066	0.068	0.065	0.066	0.063	0.068
	RMSE	0.143	0.125	0.124	0.114	0.116	0.119	0.114	0.112	0.111	0.109	0.108	0.110

Table 6

U-value obtained in the three case studies of testing.

Case study	Period	$U_{\text{Estimated}}$ [a]	Without post-processing			With post-processing		
			U_{THM} [b]	$U_{\text{THM,Fk}}$ [c]	$U_{\text{THM,MLP,Fk}}$ [d]	U_{THM} [b]	$U_{\text{THM,Fk}}$ [c]	$U_{\text{THM,MLP,Fk}}$ [d]
CS-A	*P1*	1.10	1.01 ± 0.09	1.10 ± 0.09	1.31 ± 0.07	0.59 ± 0.07	0.65 ± 0.07	1.26 ± 0.06
CS-B	*P2*	0.79	1.26 ± 0.05	1.50 ± 0.04	0.80 ± 0.07	0.99 ± 0.04	1.14 ± 0.04	0.80 ± 0.07
CS-C	*P3*	0.58	1.35 ± 0.09	1.33 ± 0.07	0.46 ± 0.04	0.17 ± 0.07	0.14 ± 0.07	0.47 ± 0.04

[a] *U*-value estimated according to the calculation procedure from ISO 6946 [27].

[b] *U*-value obtained from Eq. (4).

[c] *U*-value obtained from Eq. (12).

[d] *U*-value obtained from the MLP.